Automatic Segmentation of Femur Bones in Anterior-Posterior Pelvis X-Ray Images

Feng Ding[1], Wee Kheng Leow[1], and Tet Sen Howe[2]

[1] Dept. of Computer Science, National University of Singapore,
3 Science Drive 2, Singapore 117543
{dingfeng,leowwk}@comp.nus.edu.sg
[2] Dept. of Orthopaedics, Singapore General Hospital,
Outram Road, Singapore 169608
tshowe@sgh.com.sg*

Abstract. Segmentation of femurs in Anterior-Posterior x-ray images is very important for fracture detection, computer-aided surgery and surgical planning. Existing methods do not perform well in segmenting bones in x-ray images due to the presence of large amount of spurious edges. This paper presents an atlas-based approach for automatic segmentation of femurs in x-ray images. A robust global alignment method based on consistent sets of edge segments registers the whole atlas to the image under joint constraints. After global alignment, the femur models undergo local refinement to extract detailed contours of the femurs. Test results show that the proposed algorithm is robust and accurate in segmenting the femur contours of different patients.

1 Introduction

Segmentation of bones in medical images is very important for medical applications such as quantitative analysis [1,2,3], fracture detection [4,5], computer-aided surgery and surgical planning [6,7]. It has been performed on various types of medical images such as CT [6,8], MR [9], and x-ray [1,2,3,5,7]. Segmentation of bones in CT and MR are easier than that in x-ray images because bones have clearer boundaries in CT and MR. In contrast, segmentation of bones in x-ray images is a very difficult and challenging task that is not well solved. For example, in an anterior-posterior pelvis x-ray image, the femurs are overlapped by other body parts such as the pelvis bone, the thigh muscles, etc. As a result, some boundary edges of the femurs may be obscured while others may appear to be connected to the boundary edges of other body parts (Fig. 3). Moreover, the region within a femur's boundary has inhomogeneous image features. These difficulties render general segmentation methods such as thresholding and region-based methods inappropriate.

This paper presents an atlas-based approach for automatic segmentation of femurs in x-ray images. The atlas describes not only the femurs but also the pelvis

* This research is supported by NMRC/0482/2000.

W.G. Kropatsch, M. Kampel, and A. Hanbury (Eds.): CAIP 2007, LNCS 4673, pp. 205–212, 2007.

and the joints between them. The segmentation algorithm consists of two stages: global alignment (Section 4) and local refinement (Section 5). A robust method globally aligns the model of each bone in the atlas to the edges in the image subject to joint constraint. The pelvis and femur models constrain each other's position and orientation, making the algorithm more robust against supurious features in the image. After global alignment, a level set method with shape constraint is applied to deform the femur models to extract detailed contours of the femurs. Compared to existing segmentation algorithms, this approach is more robust and accurate in segmenting the femur contours of different patients.

2 Related Work

Existing medical image segmentation methods fall into several categories [10]. Region-based methods assume intra-region homogeneity, and usually produce over-segmented results. Classfication-based methods do not consider spatial information. Therefore, the segmented regions are disjoint. Deformable model-based algorithms need good initialization. The deformation needs to be well controlled to prevent leakage. In comparison, atlas-based methods [7,8,11,12], which register reference atlases to the target images, are more promising because the atlases contain domain knowledge that guides the segmentation process.

For femur segmentation in x-ray images, the method of Chen *et al.* [5] segments femurs by first detecing parallel lines in the shaft region and circles in the femoral heads to initialize a 2D model. The model is then deformed by a snake algorithm with curvature constraint. Spurious edges can affect the initialization of the snake model, and attract the snake towards them.

The method of Boukala *et al.* [7] segments pelvis and femurs in AP x-ray images. It registers the mean shape of the training samples to the input image by explicitly finding correspondence using shape context descriptor [13], which is a log-polar edge point histogram. Active shape model is applied to deform the registered atlas to extract detailed bone contours. Note that randomly located spurious edges in the image may cause edge points counting in shape context to fail. This problem is very serious for AP x-ray images due to the presence of large amount of spurious edges. As a result, it will lead to incorrect correspondence.

In contrast, the proposed algorithm does not rely only on feature matching to determine correspondence from the atlas contours to the extracted edges. Instead, it generates multiple possible matches and adopts a robust method to identify the more likely candidates based on consistent sets of edge segments. Level set method with shape constraint is used to deform the aligned atlas to extract detailed femur contours.

3 Pelvis Atlas

Our approach constructs an atlas that captures not only the femurs but also the pelvis and the joints that connect them (Fig. 1(c)). Each bone model is constructed from 20 manually segmented training samples that are represented

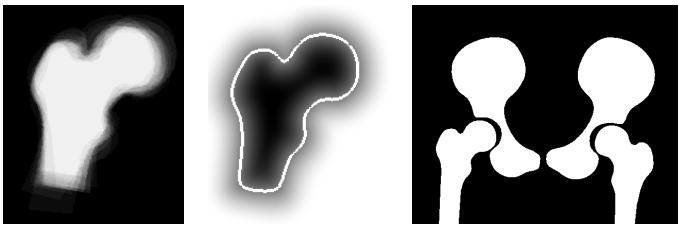

(a) (b) (c)

Fig. 1. Pelvis atlas. (a) Superposition of 20 aligned training samples. (b) Level set representation of the mean shape. White curve: zero level set. (c) Constructed atlas.

as level set functions (signed distance maps, Fig. 1(b)). The shaft regions of these samples are cut to the same length. These samples are automatically aligned under rigid transformations by maximizing their overlapping areas (Fig. 1(a)). Next, Principal Component Analysis (PCA) is applied to compute the eigenshapes of the model. The mean shapes of femurs are then connected to that of the pelvis at the joint positions (Fig. 1(c)). The shafts of the femur model are extended for matching long femurs in the images.

4 Global Alignment

The goal of global alignment is to align the model's position and orientation to match the bones in the image. The scale ratio is assumed to be approximately 1. Each of the three model contours of the bones (two femurs and one pelvis) in the atlas needs to be aligned under a different rigid transformation subject to the joint constraints because the femurs can rotate about the joints.

The algorithm contains four main stages:

1. Extraction of edge segments from the input x-ray image.
2. Estimation of possible correspondence between model contours and edge segments.
3. Determination of a consistent set of edge segments that correspond to each model contour.
4. Compute transformations and register each model contour to the image.

These stages are discussed in the following sections.

4.1 Edge Segment Extraction

Histogram equalization is first applied to the input image to roughly normalize the intensity and contrast of the image. Next, edges are extracted from the normalized image using Canny edge detector, and edge direction at each edge point is computed. Finally, connected edge points are joined to form edge segments. Edge segments that are too short are regarded as noise and discarded.

4.2 Estimation of Possible Correspondence

This stage determines the possible correspondence between the edge segments and the bone models. Let e denote an edge segment with edge points $\mathbf{p}_i$, $i = 1, \ldots, m$, whose edge directions are given by the unit vectors $\mathbf{u}_i$. Let c denote a model contour of a bone with contour points $\mathbf{q}_j$, $j = 1, \ldots, n$ and contour directions $\mathbf{v}_j$. If c is a closed contour, then $\mathbf{q}_{n+1} = \mathbf{q}_1$. As an edge segment of a bone may contain edge points that do not correspond to the model contour, the objective of this stage is to find the longest sub-sequence $e' = e(a, l) = (\mathbf{p}_a, \ldots, \mathbf{p}_{a+l})$ of e that corresponds to a sub-sequence $c' = c(b, l) = (\mathbf{q}_b, \ldots, \mathbf{q}_{b+l})$ of c, for some a and b, where l is the length of the sub-sequence. If c is an open contour, then the following boundary condition holds for the longest corresponding sub-sequences e' and c': either (1) $\mathbf{p}_a = \mathbf{p}_1$ and $\mathbf{q}_{b+l} = \mathbf{q}_n$ or (2) $\mathbf{p}_{a+l} = \mathbf{p}_m$ and $\mathbf{q}_b = \mathbf{q}_1$. Otherwise, the longest $e' = e$.

The similarity $s(e', c')$ between e' and c' is defined in terms of three factors:

$$s(e', c') = \eta(e', c')\rho(e', c')\psi(e', c'). \tag{1}$$

The global direction similarity $\eta(e', c')$ measures the overall directional alignment between e' and c' based on the global direction vectors $\boldsymbol{\theta}$ of e' and c':

$$\eta(e', c') = \begin{cases} \exp[-\lambda_1(1 - \boldsymbol{\theta}(e') \cdot \boldsymbol{\theta}(c'))] & \text{if } \boldsymbol{\theta}(e') \cdot \boldsymbol{\theta}(c') > \tau \\ 0 & \text{otherwise} \end{cases} \tag{2}$$

where τ is a threshold, and λ_1 is a constant parameter. The global direction $\boldsymbol{\theta}(e')$ of e' (similarly for c') is estimated by the mean of its edge point directions: $\boldsymbol{\theta}(e') = \sum_{i=a}^{a+l} \mathbf{u}_i/(l+1)$.

The local direction similarity $\rho(e', c')$ measures the degree of match between the edge point directions of e' and c'. It is computed as the similarity between their edge point directions relative to their global directions:

$$\rho(e', c') = \frac{1}{l+1} \sum_{i=a}^{a+l} (\mathbf{u}_i - \boldsymbol{\theta}(e')) \cdot (\mathbf{v}_{f(i)} - \boldsymbol{\theta}(c')) \tag{3}$$

where f is a mapping function that maps $\mathbf{p}_i$ to $\mathbf{q}_j$, i.e., $j = f(i)$.

The local position similarity $\psi(e', c')$ measures the degree of match between the positions of the edge points of e' and c':

$$\psi(e', c') = \exp\left[-\frac{\lambda_2}{l+1} \sum_{i=a}^{a+l} \|\mathbf{p}_i - \mathbf{q}_{f(i)}\|^2\right]. \tag{4}$$

where λ_2 is a constant parameter.

Given the similarity $s(e', c')$, the longest best matching sub-sequences of e and c are the pair $e(a^*, l^*)$ and $c(b^*, l^*)$ that maximize the sub-sequence similarity:

$$s(e(a^*, l^*), c(b^*, l^*)) = \max_{a,b,l} s(e(a, l), c(b, l)). \tag{5}$$

4.3 Determination of Consistent Sets

The previous stage will find many possible corresponding edge segments for each model contour. Some of them are correct correspondences while the others are not. Since the bone is rigid, it must be possible to register the model contour to a set of consistent edge segments under the same rigid transformation.

Let e'_k correspond to sub-sequence c'_k of c. The rigid transformation T_k from c'_k to e'_k is computed using the algorithm in [14]. The computed transformation T_k is then applied to the whole model contour c. Two transformations T_i and T_k on c are consistent if they produce similar transformations of c:

$$d(c, T_i, T_k) = \frac{1}{|c|} \sum_{\mathbf{q}_j \in c} \|T_i(\mathbf{q}_j) - T_k(\mathbf{q}_j)\|^2. \tag{6}$$

The smaller the d, the more consistent are the transformations. Given a set $S(c)$ of edge segments e'_k for model contour c with associated transformations T_k, the overall consistency of the set is then defined by the maximum difference $D(S)$:

$$D(S(c)) = \max_{e'_i, e'_k \in S(c)} d(c, T_i, T_k). \tag{7}$$

The smaller the D, the more consistent is the set. Given a consistent set $S(c)$, the overall transformation T between c and every $e'_k \in S(c)$ is computed using the algorithm in [14]. For each model contour, multiple consistent sets are sampled using RANSAC [15], each having an overall transformation (Fig. 2). So a model contour c has a set $\Gamma(c)$ of possible transformations that map c to consistent sets of edge segments.

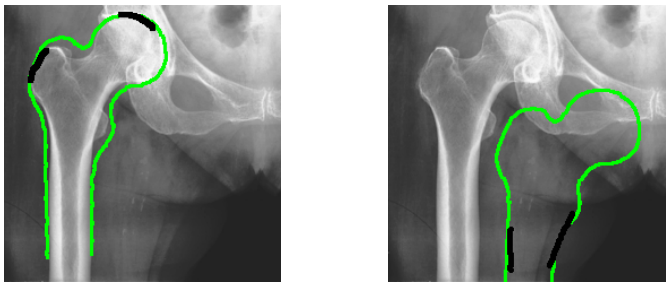

(a) (b)

Fig. 2. Determine optimal transformations. (a) Correct correspondence of edge segments (black line) leads to registration (green) with small registration error. (b) Incorrect correspondence leads to incorrect registration with large error.

4.4 Computation of Optimal Transformations

This step computes the optimal transformation for each model contour c subject to joint constraints. Let J denote a set of joints and $\mathbf{x}(c_r, c_s) \in J$ denote the position where model contour c_r and c_s are connected to form a joint. The joint constraint is satisfied if the penalty P is small:

$$P = \sum_{\mathbf{x}(c_r,c_s)\in J} \|T_r(\mathbf{x}(c_r,c_s)) - T_s(\mathbf{x}(c_r,c_s))\|^2 \tag{8}$$

for some $T_r \in \Gamma(c_r)$ and $T_s \in \Gamma(c_s)$. The registration error R measures the degree of match between the models and the edges in the image:

$$R = \sum_{r=1}^{M} \sum_{\mathbf{q}_j \in c_r} \|T_r(\mathbf{q}_j) - g(\mathbf{q}_j)\|^2 \tag{9}$$

where M is the number of model contours and $g(\mathbf{q}_j)$ is the closest edge point in the image to $\mathbf{q}_j$. So, the optimal transformations of the models are obtained by determining the optimal T_r from the set $\Gamma(c_r)$ of each model c_r that together minimize the total error E:

$$E = R + \lambda_3 P \tag{10}$$

where λ_3 is a weighting parameter. Fig. 3(a) shows a global alignment result.

5 Local Refinement

This stage deforms the globally aligned model contours to register to the femurs in the image. It iteratively evolves a level set function under dynamic directional gradient vector flow (DDGVF) [16] subject to statistical shape constraint. DDGVF is an extension of GVF that computes GVF in both the positive and negative directions. It is originally proposed as an image force in the snake framework. In our algorithm, it is incorporated into the level set framework. When the level set function is evolving, only those edges having similar edge directions as the zero level set will contribute to the GVF. This allows the final zero level set to have the same edge point directions as the edges that attract it.

The shape constraint is incorporated into the level set function based on the method in [17]. In each iteration, the level set function is updated according to the linear combination of DDGVF, curvature and shape constraint as follows:

$$\phi(t+1) = \phi(t) + \alpha_1 F \cdot \nabla\phi(t) + \alpha_2 \nabla \cdot \frac{\nabla\phi(t)}{|\nabla\phi(t)|} + \alpha_3(\phi^*(t) - \phi(t)) \tag{11}$$

where F is the force produced by DDGVF, ϕ^* is the maximum *a posterori* (MAP) shape estimated based on the training samples, and α_i are weighting parameters. The evolution of the level set is guided by the DDGVF term, kept smooth by the curvature term, and does not deform the shape too drastically. A sample local alignment result is shown in Fig. 3(b).

6 Experiment and Discussion

An experiment was performed to evaluate the accuracy of the atlas-based algorithm. The test set contained another 20 AP pelvis images of different patients,

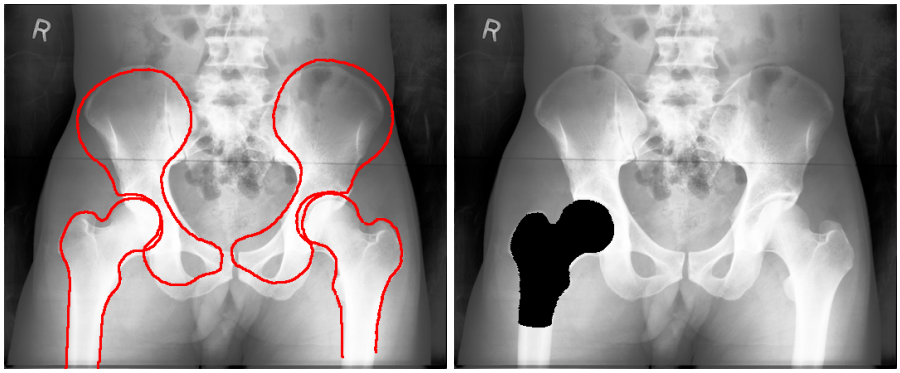

(a) (b)

Fig. 3. Sample results. (a) Global alignment result (red curve). (b) Segmented femur (black region) after local refinement.

Table 1. Quantitative segmentation results

Image No.	1	2	3	4	5	6	7	8	9	10
RMSD	3.90	3.60	3.46	2.50	1.77	3.99	2.77	3.97	2.80	3.74
Image No.	11	12	13	14	15	16	17	18	19	20
RMSD	3.26	3.10	2.17	1.53	1.68	3.91	1.69	2.70	4.57	3.28

including both males and females. Test results show that on average, each femur contains 7 consistent sets, and each set contains 2 edge segments. For pelvis, the numbers are 7 and 3 respectively.

The root-mean-squared distances (RMSD) (in pixel) between the segmented femur contours and the manually segmented ground truth were computed (Table 1). The average RMSD is 3.02 with standard deviation of 0.90. Compared to the image size of 534×440, an error of 3 pixels can be considered very accurate.

The segmentation problem becomes very challenging if the femur bones to be segmented are fractured. For minor (hairline) fractures, the proposed algorithm can still work since the femurs' shapes are unchanged. It is extremely difficult if femurs to be segmented contain major fractures, i.e., not only the shapes but also the topologies of femur contours can change. This problem requires further research.

7 Conclusion

This paper presents an atlas-based approach for automatic segmentation of femurs in x-ray images. The atlas describes the femurs, the pelvis, and the joints that connect them. A robust method globally aligns the atlas to the input image by generating multiple possible matches, and identifying the more likely candidates based on consistent sets of edge segments. Level set method deforms the aligned atlas to

extract detailed femur contours. Test results show that the proposed algorithm is robust and accurate in segmenting the femur contours of different patients.

References

1. Manos, G.K., Cairns, A.Y., Rickets, I.W., Sinclair, D.: Segmenting radiographs of the hand and wrist. Computer Methods and Programs in Biomedicine 43(3-4), 227–237 (1993)
2. Chen, H., Jain, A.K.: Tooth contour extraction for matching dental radiographs. In: Proc. Int. Conf. on Pattern Recognition, pp. 522–525 (2004)
3. El-Feghi, I., Huang, S.S.A., M.A., Ahmadi, M.: X-ray image segmentation using auto adaptive fuzzy index measure. In: Proc. Midwest Symposium on Circuits and Systems. vol. 3, pp. 499–502 (2004)
4. Yap, D.W.H., Chen, Y., Leow, W.K., En Howe, T.: Detecting femur fractures by texture analysis of trabeculae. In: Proc. Int. Conf. on Pattern Recognition 3, 730–733 (2004)
5. Chen, Y., Ee, X., Leow, W.K., Howe, T.S.: Automatic extraction of femur contours from hip x-ray images. In: Proc. ICCV Workshop on Computer Vision for Biomedical Image Applications, pp. 200–209 (2005)
6. Dammann, F., Bode, A., Schwaderer, E., Schaich, M., Heuschmid, M., Maassen, M.M.: Computer-aided surgical planning for implantation of hearing aids based on ct data in a vr environment. Radiographics 21, 183–190 (2001)
7. Boukala, N., Favier, E., Laget, B., Radeva, P.: Active shape model based segmentation of bone structures in hip radiographs. In: Proc. of IEEE Int. Conf. on Industrial Technology, pp. 1682–1687 (2004)
8. Duay, V., Houhou, N., Thiran, J.P.: Atlas-based segmentation of medical images locally constrained by level sets. Technical report, Signal Processing Institute (ITS), Ecole Polytechnique Fédérale de Lausanne (EPFL) (2005)
9. Cootes, T.F., Taylor, C.J.: Statistical models of appearance for computer vision. Technical report, Imaging Science and Biomedical Engineering, Manchester M13 9PT, U.K. (2004)
10. Pham, D.L., Xu, C., Prince, J.L.: A survey of current methods in medical image segmentation. Technical report, Department of Electrical and Computer Engineering, The Johns Hopkins University (1998)
11. Ding, F., Leow, W.K., Wang, S.C.: Segmentation of 3D CT volume images using a single 2D atlas. In: Proc. ICCV Workshop on Computer Vision for Biomedical Image Applications, pp. 459–468 (2005)
12. Vinhais, C., Campilho, A.: Genetic model-based segmentation of chest x-ray images using free form deformations. In: Proc. Int. Conf. Image Analysis and Recognition. (2005)
13. Belongie, S., Malik, J., Puzicha, J.: Shape context: A new descriptor for shape matching and object recognition. In: NIPS, pp. 831–837 (2000)
14. Jain, R., Kasturi, R., Schunck, B.G.: Machine Vision. McGraw-Hill, New York (1995)
15. Fischler, M.A., Bolles, R.C.: Random sample consensus: A paradigm for model fitting with applications to image analysis and automated cartography. ACM 24(6), 381–395 (1981)
16. Cheng, J., Foo, S.W.: Dynamic directional gradient vector flow for snakes. IEEE Trans.on Image Processing 15(6), 1563–1571 (2006)
17. Leventon, M.E., Grimson, W.E.L., Faugeras, O.: Statistical shape influence in geodesic active contours. In: Proc. CVPR. vol. 1, pp. 316–323 (2000)